ISSN 1063-7710, Acoustical Physics, 2025, Vol. 71, No. 3, pp. 346–356. © The Author(s), 2025. This article is an open access publication.

NONLINEAR ACOUSTICS

Effect of the Diameter of the Central Opening on Nonlinear Acoustic Field Characteristics of High-Intensity Focused Ultrasound Transducers

F. A. Nartov[a], *, M. M. Karzova[a], and V. A. Khokhlova[a]

[a] *Moscow State University, Faculty of Physics, Moscow, 119991 Russia*

**e-mail: nartov.fyodor@gmail.com*

Received September 4, 2024; revised February 28, 2025; accepted May 6, 2025

Abstract—A number of novel noninvasive surgical technologies utilizing high-intensity focused ultrasound (HIFU) are based on using nonlinear acoustic effects that lead to distortion of the wave when it propagates from an ultrasound transducer and formation of shock fronts at the focus. Typically, such transducers that generate a high-power ultrasound beam, have near axially symmetric shape with a central circular opening to accommodate a diagnostic probe for visualization purposes. To predict the focal field parameters of such transducer geometries, an equivalent source model of a spherical segment is convenient, as nonlinear effects in its field are well studied. The equivalent source parameters (diameter, focal length, and amplitude) are optimized to closely approximate the focal region of the original transducer along the axial coordinate. This paper investigates the effect of the central opening size on the nonlinear field characteristics and applicability of the equivalent source model for a typical therapeutic ultrasound transducer with a frequency of 1 MHz and $F_{\#} = 0.9$. It is demonstrated that the size of the central opening significantly affects the degree of nonlinear waveform distortion in the focal region, and the equivalent source model can be applied only when the diameter of the central opening is less than 20% of the transducer diameter.

Keywords: HIFU, nonlinear effects, diffraction, shock fronts, equivalent source

DOI: 10.1134/S1063771024602681

INTRODUCTION

In recent years, novel medical applications of high-intensity focused ultrasound (HIFU) based on the use of nonlinear acoustic effects were actively developing [1–4]. One example is the HIFU noninvasive surgical technology, in which ultrasound is focused on the target site of inducing an intended therapeutic effect, followed by its thermal or mechanical destruction [3–5]. To achieve thermal destruction of biological tissue, both weakly nonlinear and shock-wave sonication modes have been used [6–9]. To create mechanical tissue destruction, histotripsy methods have been developed, which employ shock-wave pulse-periodic sonication modes with a low duty cycle [3, 4, 10].

Modern HIFU transducers are often multielement arrays, the elements of which are located on a spherical segment with a central opening that holds a diagnostic probe for visualization of the effect [11–17]. In this case, the shape of the elements, as well as their location on the surface, can be different. For example, the phased arrays of the Sonalleve clinical HIFU system (Profound Medical Corp., Canada) comprise 256 circular elements, randomly distributed on a spherical surface in the case of the V1 model and on eight sectors of the spherical surface in the case of the V2 model [13]; a similar randomized design was also used previously [12]. The prototype of the system for treatments of abdominal organs using boiling histotripsy has a transducer in the form of a phased 256-element array, in which the circular elements are located on 16 spirals extending from the edge of the opening [11]. There are transducers with sector geometry [14], with dense mosaic filling of elements in the form of polygons [15], with an arrangement of seven circular elements in the shape of a daisy [16]. Despite the differences in the shape of the elements and their arrangement around the central circular opening, such transducers generate acoustic fields that are close in structure to axially symmetric ones.

For the most accurate acoustic characterization of nonlinear fields generated by such transducers, a comprehensive approach based on complementary data from physical and numerical experiments has been developed and successfully applied [11, 13, 16–21]. To set a boundary condition in numerical modeling, acoustic holography method is used, in which spatial distributions of amplitudes and phases of the ultrasound field are measured in a plane perpendicular to the acoustic beam axis [19]. Measurements are carried out in the linear propagation regime with the trans-

ducer operating at low power output. Next, based on the experimental holography data, spatial distribution of the vibrational velocity on the surface of the transducer is calculated using the Rayleigh integral. The boundary condition obtained in this way is scaled in amplitude and used to numerically model the three-dimensional Westervelt equation within a wide range of power levels supplied to the transducer [11, 13, 16–22]. With this method, one can determine the parameters of nonlinear ultrasound field in the entire volume of the focused beam; however, modeling of the three-dimensional Westervelt equation requires large computational resources and is not yet widely available today [23].

In many cases, when it is sufficient to know the field parameters only in the focal region of the beam, a simpler equivalent source model is applicable, which allows the use of existing open-access numerical algorithms for modeling axially symmetric beams [24, 25]. The principle of constructing an equivalent source model is as follows: an equivalent source in the form of a spherical segment with a uniform distribution of vibrational velocity over its surface is selected in accordance with the real transducer in such a way that, in the case of linear propagation, the axial distributions of the pressure amplitude in the vicinity of the focal maximum for the real transducer and the equivalent source match each other in the best possible way [17, 26]. In some cases, the correspondence between the pressure amplitude in the focal region, determined at a certain level from the maximum in the analytical solution for the equivalent source and calculated from the acoustic holography data for the original transducer, is used [27–29]. In other cases, it is possible to achieve coincidence of the pressure amplitude at the focus, the position of the zeros closest to the focus, and the pressure amplitude distributions between them [13, 17]. Since for highly focused transducers nonlinear effects are most pronounced in the focal region, where the field amplitude is the highest, and in the prefocal region the beam propagates almost linearly, it is assumed that the selected equivalent source model, when scaling its power, will govern the field in the focal region of a real transducer also in the case of nonlinear propagation, including the formation of shock fronts in the focal profile of the wave [17, 26].

Indeed, recent studies have shown that the equivalent source model governs with good accuracy the shock-wave fields generated by multielement phased therapeutic HIFU arrays and sector transducers [11, 13, 17, 20, 28, 29]. The simplicity of using the equivalent source model is that to construct it, it is sufficient to know only the one-dimensional distribution of the linear field along the beam axis in the focal region of the transducer. Then modeling the nonlinear field created by the selected equivalent source is conveniently carried out using open-access software packages, e.g., in "HIFU beam" [25]. It is important to note that the results of previous numerical experiments for transducers with different values of the focusing angle and aperture, measured in wavelengths of the transducer's operating frequency, are also available [17].

As mentioned above, many of the modern high-power focused ultrasound transducers have an opening in the center, which is used to accommodate a diagnostic ultrasound probe [11, 13, 17, 20, 28, 29]. In one of the recent studies on the acoustic characterization of the field of a 256-element phased therapeutic array of the MR-HIFU Sonalleve V2 system (Profound Medical Corp., Canada) with a central opening of a sufficiently large size (opening diameter 40 mm, outer diameter of the transducer 136 mm), it was shown that the equivalent source model, when simulating nonlinear effects, underestimates the level of peak positive pressure in shock-wave focusing modes by up to 20% compared to the real field [13]. Moreover, for a similar Sonalleve therapeutic array of the previous model V1 with a central opening diameter twice smaller than that of the V2 model and similar other parameters, the equivalent source model governs with high accuracy (difference less than 5%) the values of peak positive and negative pressures in the focal wave profile in the entire range of array operating power levels (up to 1.1 kW of acoustic power) [13, 20]. Thus, in [13] it was demonstrated that if the central opening of the transducer is sufficiently large, the equivalent source model does not provide acceptable accuracy. In order to achieve it, it is necessary to conduct modeling taking into account a central opening of the same diameter as in the real transducer. Such model of the transducer in the form of a segment of a sphere with a central opening made it possible to predict the parameters of the nonlinear field at the focus of the V2 array much more accurately (the difference is less than 5%) compared to the model of an equivalent source.

The aim of this study was to quantify the effect of the size of the central opening on the degree of nonlinear effects in the focal region of the transducer and to estimate the maximum values of the opening diameter at which the equivalent source model can be considered applicable. A transducer with a frequency of 1 MHz, aperture of 100 mm, and focal length of 90 mm, typical for existing ultrasound surgery systems, was considered as an example. In the numerical experiment, cases of openings with diameters within the range from 10 to 70 mm with a step of 10 mm were investigated. The differences in the spatiotemporal structure of the nonlinear acoustic field of the transducer and the corresponding equivalent source, which appear as the size of the central opening increases, were analyzed (Fig. 1). Nonlinear effects were modeled in a wide range of the transducer's acoustic power: from linear focusing to the formation of the developed shock in the wave profile at the focus, and reaching the saturation regime [17].

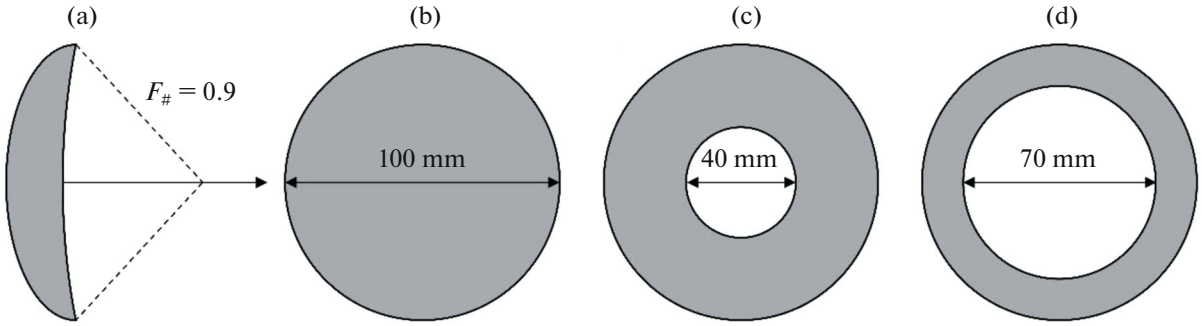

Fig. 1. (a) Model of a spherical transducer with $F_\# = 0.9$ (side view); models of spherical transducers with different sizes of central opening (front view): (b) 0, (c) 40, (d) 70 mm.

NUMERICAL MODEL

1. Linear Field

Modeling of the acoustic field generated by transducers (Fig. 1) operating in the linear ultrasound propagation conditions was performed using the Rayleigh integral assuming a uniform distribution of the normal component of the vibrational velocity v_n over the active surface Σ of the transducer [19]:

$$p(x,y,z) = -\frac{i\omega\rho_0}{2\pi}\int\limits_{\Sigma} v_n(x_1,y_1,z_1)\frac{e^{ikR}}{R}d\Sigma, \qquad (1)$$

where $p(x,y,z)$ is the complex pressure amplitude at the observation point with coordinates (x,y,z), (x_1,y_1,z_1) are the coordinates of the transducer surface element, $R = \sqrt{(x-x_1)^2+(y-y_1)^2+(z-z_1)^2}$ is the distance between the surface element and the observation point, $k = 2\pi f/c_0$ is the wave number, f is the ultrasound radiation frequency, c_0 is the sound speed in the propagation medium, ρ_0 is the density of the propagation medium.

The analytical solution of the Rayleigh integral (1) for the distribution of the complex pressure amplitude along the z axis of a transducer in the form of a spherical segment with a radius of curvature F and an aperture D has the form

$$p(r=0,z) = p_0\frac{e^{ikz} - e^{ikR_{\max}}}{1 - z/F}, \qquad (2)$$

where r is the transverse coordinate measured from the z axis, $p_0 = \rho_0 c_0 v_0$ is the characteristic pressure amplitude at the source, v_0 is the amplitude of the vibrational velocity at the surface of the transducer, $R_{\max} = F\sqrt{1+(1-z/F)^2 - 2(1-z/F)\cos\alpha_{\max}}$ is the distance from the observation point to the edge of the transducer, $\alpha_{\max} = \arcsin(a/F)$ is the convergence angle, $a = D/2$ is the radius of the transducer [19]. Alternatively, to characterize the convergence angle of the ultrasound beam, a dimensionless parameter is often used, equal to the ratio of the focal length of the transducer to its diameter (the F-number): $F_\# = F/D$ [17]. For the transverse distribution of the pressure amplitude along the axis r in the focal plane $z = F$ of the transducer in the form of a spherical segment, the approximate solution of the Rayleigh integral (1) has the form:

$$p(r,z=F) = p_0 kF\frac{\alpha_{\max}^2}{2}\left|\frac{2J_1(kr\alpha_{\max})}{kr\alpha_{\max}}\right|, \qquad (3)$$

where J_1 is the Bessel function of the 1st kind and 1st order [30].

In the case of a spherical transducer with a central opening of diameter d, the distribution of the pressure amplitude along the beam axis z due to the linearity of the problem, can be found as the difference between solutions (2) for a transducer with an aperture of D without a central opening and a transducer with an aperture equal to the diameter of the central opening d. Similarly, the transverse distribution of the pressure amplitude in the focal plane $z = F$ can also be calculated analytically as the difference of solutions (3) for transducers with apertures D and d.

2. Nonlinear Field

For nonlinear modeling, we used a "HIFU beam" software package based on the solution to the Westervelt equation for axially symmetric focused beams [25]:

$$\frac{\partial^2 p}{\partial\tau\partial z} = \frac{c_0}{2}\left(\frac{\partial^2 p}{\partial z^2} + \frac{\partial^2 p}{\partial r^2} + \frac{1}{r}\frac{\partial p}{\partial r}\right) + \frac{\varepsilon}{2\rho_0 c_0^3}\frac{\partial^2 p^2}{\partial\tau^2} + \frac{\delta}{2c_0^3}\frac{\partial^3 p}{\partial\tau^3}, \qquad (4)$$

where $\tau = t - z/c_0$ is the retarded time, t is time, ε is the nonlinearity coefficient, δ is the thermoviscous absorption coefficient. In the context of the problem considered here, the physical parameters of the propagation medium corresponded to the parameters of

water at a temperature of 20°C: $c_0 = 1485$ m/s, $\rho_0 = 997$ kg/m^3, $\varepsilon = 3.5$, $\delta = 4.33 \times 10^{-6}$ m^2/s [13].

In the simulations, the grid step along the axial coordinate z was $h_z = 0.025$ mm, and the step along the radial coordinate r was $h_r = 0.05$ mm. For calculations at high power levels of the transducer, the step along the r axis was reduced by four times to avoid Gibbs oscillations in the wave profile.

ALGORITHM FOR CONSTRUCTING AN EQUIVALENT SOURCE MODEL

The first step in constructing an equivalent source model is to find the spatial distribution of the pressure amplitude along the axial coordinate z in the focal region of the original transducer. In this paper, the analytical solution of the Rayleigh integral (2) was used to obtain this distribution. In the case where an equivalent source is constructed for a real physical transducer, the axial distribution of the pressure amplitude is determined either using its nominal dimensions or, more accurately, based on the hydrophone measurements under the condition of linear wave propagation at low radiated power [13, 16, 20, 29].

The second stage is to find the parameters of the equivalent source, including the aperture, focal length, and wave amplitude on the transducer, in such a way that the axial distribution of the pressure amplitude for the selected equivalent source in the region of the main focal lobe provides the best match with the corresponding distribution for the original transducer. In the case of the transducers selected in this study with a uniform vibrational velocity distribution on a spherical surface in the form of a ring, the equivalent source parameters can be calculated analytically, based on the condition that the amplitude of the field at the focus and positions of the zeros closest to the focus (in front of and behind it) along the transducer axis coincide for the original transducer and the equivalent source [17, 26].

It can be shown that a sufficient condition for meeting these requirements for a transducer with a central opening and its equivalent source is the equality of the focal lengths F, characteristic initial pressure amplitudes $p_0 = \rho_0 c_0 v_0$, and areas of their operating surfaces. Indeed, according to the solution (2), the distribution of the pressure amplitude along the axis of the equivalent source has the form

$$A_{\text{eq}}(r=0,z) = \frac{2p_0}{\delta}\left|\sin\left(k\frac{z-R_{\max,\text{eq}}}{2}\right)\right|, \qquad (5)$$

where $R_{\max,\text{eq}} = F\sqrt{1+(1-z/F)^2-2(1-z/F)\cos\alpha_{\max,\text{eq}}}$ is the distance from the observation point to the edge of the equivalent source, $\alpha_{\max,\text{eq}} = \arcsin(a_{\text{eq}}/F)$, $\delta = 1 - z/F$, $k = 2\pi f/c_0$ is the wave number, and f is the ultrasound frequency. The corresponding pressure amplitude distribution for a spherical transducer with a central opening can be written as

$$A(r=0,z) = \frac{2p_0}{\delta}\left|\sin\left(k\frac{R_{\max 1}-R_{\max 2}}{2}\right)\right|. \qquad (6)$$

The condition of coincidence of the zeros closest to the focus in the solutions (6) and (7) is the condition when the sine arguments become equal to $\pm\pi$:

$$k\frac{F(1-\delta)-R_{\max,\text{eq}}}{2} = k\frac{R_{\max 1}-R_{\max 2}}{2} = \pm\pi, \qquad (7)$$

or

$$F(1-\delta)-R_{\max,\text{eq}} = R_{\max 1}-R_{\max 2}. \qquad (8)$$

Considering that $\delta \ll 1$ near the focus, the expansion of the solutions for $R_{\max}$ into a Taylor series in δ at the point $\delta = 0$ up to the first-order accuracy, $R_{\max} = F(1-\delta\cos\alpha_{\max})$, and further substitution into the solution (8), yields

$$1-\cos\alpha_{\max,\text{eq}} = \cos\alpha_{\max 1}-\cos\alpha_{\max 2}. \qquad (9)$$

Here $\alpha_{\max,\text{eq}} = \arcsin(a/F)$ is the angle between the axis of the equivalent source and the direction to its outer edge from the point of the geometric focus, $\alpha_{\max 1,2} = \arcsin(a_{1,2}/F)$ represents the angles between the axis of the ring transducer and the direction to its inner and outer edges from the geometric focus point, respectively.

Note that the condition (9) is met if the areas of the equivalent source $S_{\text{eq}} = 2\pi F^2(1-\cos\alpha_{\max,\text{eq}})$ and the spherical segment with a central opening $S = 2\pi F^2(\cos\alpha_{\max 1}-\cos\alpha_{\max 2})$ are equal. This automatically ensures meeting the third condition of equal pressure amplitudes at the focus for equal the pressure amplitudes p_0 on the surfaces of the equivalent source

$$p_{\text{eq},F} = p_0 kF(1-\cos\alpha_{\max,\text{eq}}) = p_0 f S_{\text{eq}}/(c_0 F) \qquad (10)$$

and a spherical transducer with a central opening:

$$p_F = p_0 kF(\cos\alpha_{\max 1}-\cos\alpha_{\max 2}) = p_0 f S/(c_0 F). \qquad (11)$$

As follows from the solution (9), the radius of the equivalent source a_{eq} can be calculated as

$$a_{\text{eq}} = F\sqrt{1-(1+\cos\alpha_{\max 2}-\cos\alpha_{\max 1})^2}, \qquad (12)$$

and the distance l between the zeros of the field around the focus on the beam axis in accordance with (7) is

$$l = \frac{4\pi/k}{\cos\alpha_{\max 1}-\cos\alpha_{\max 2}} = \frac{4\pi/k}{1-\cos\alpha_{\max,\text{eq}}}. \qquad (13)$$

RESULTS

1. Linear field

Figure 2 shows the axial distributions of the pressure amplitude, normalized to the characteristic value

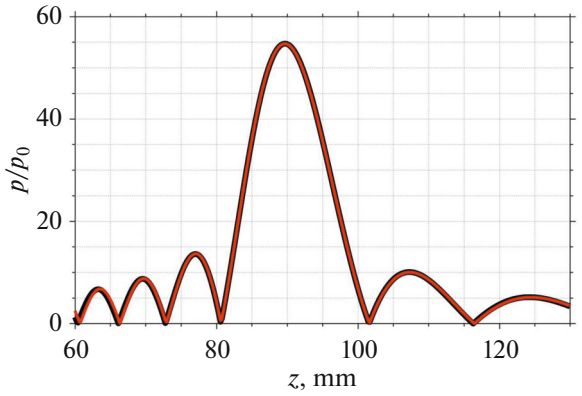

Fig. 2. Axial distributions of normalized pressure amplitude in linear beam for transducer with central opening of 40 mm in diameter: black, original transducer; red, equivalent source.

of the initial pressure $p_0 = \rho_0 c_0 v_0$, for a transducer with a central opening diameter of 40 mm and its equivalent source. The distributions are practically indistinguishable from each other not only in the region of the focal maximum, but also in several subsequent diffraction lobes before and after the focus. Thus, in the case of linear wave propagation, the condition of equal areas of the initial transducer with a central opening and the equivalent source with the same focal lengths and pressure amplitudes on the operating surface ensures matching the pressure distributions along the beam axis of these transducers in a wide range of distances (~0.3F) and positions of several field zeros around the focus (Fig. 2).

Shown in Fig. 3 are two-dimensional distributions of the normalized pressure amplitude under linear focusing conditions for transducers without an opening (Figure 3a) and with openings of 40 (Fig. 3b) and 70 mm (Fig. 3d) diameters. The distributions for each transducer with a central opening (Figs. 3b, 3d) and for the corresponding equivalent source (Figs. 3c, 3d) with the aperture calculated using (12), are shown in pairs. Accordingly, for a transducer with the parameters indicated earlier and central opening diameter of 40 mm, the equivalent source has a full aperture of 92.9 mm, and for a transducer with a 70 mm opening, the full aperture of the equivalent source is 74.6 mm. As follows from the results presented in the figure, an increase in the size of the opening and a corresponding decrease in the area of the operating surface of the transducer lead, in accordance with the solutions (2) and (3), to a decrease in the pressure amplitude at the focus. This result follows from the Rayleigh integral solution (1): the focusing gain of the pressure amplitude at the focus is proportional to the area of the operating surface of the transducer.

The size of the focal region, the boundaries of which we define at the level of –6 dB from the pressure amplitude at the focus, also changes with an increase in the size of the opening. Along the beam axis, the focal spot size was 10.6 mm for the transducer without an opening, 12.5 mm for the transducer with an opening of 40 mm in diameter, and 19.9 mm for the transducer with an opening of 70 mm in diameter. The fields of equivalent sources, as follows from their definition, had the same dimensions along the beam axis and, accordingly, the same tendency to lengthen the focal region as the central opening of the original transducer increased. However, the change of the focal region in the transverse direction, with an increase in the size of the opening, is qualitatively different for the original transducers and equivalent sources. The focal width for transducers with an opening decreases with an increase in the diameter of the opening: 1.9, 1.7 and 1.5 mm, respectively (Figs. 3a, 3b, 3d); while for equivalent sources, conversely, it increases: 1.9, 2.0, and 2.5 mm, respectively (Figs. 3a, 3c, 3d).

The observed trends in the change in the dimensions of the focal region of equivalent sources are

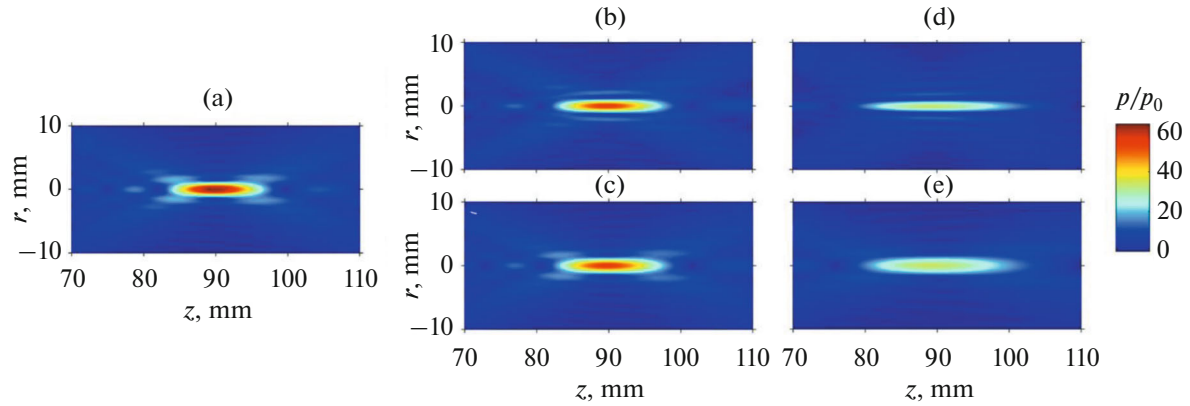

Fig. 3. Distributions of normalized pressure amplitudes in the axial plane in a focal region of the linear ultrasound beam for transducers with different central openings and their equivalent sources. (a) Transducer without an opening; upper row (b, d) – fields of original transducers; lower row (c, d) – sources equivalent to them. Aperture diameters: (a) 0, (b, c) 40, (d, e) 70 mm.

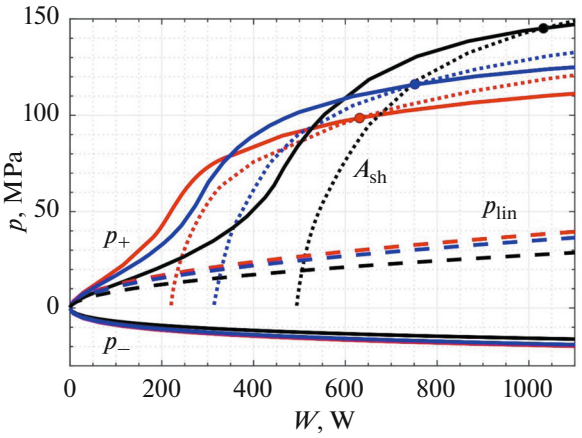

Fig. 4. Saturation curves: dependences of peak positive and peak negative pressures (solid lines) and shock amplitude (dashed lines) on transducer power for different sizes of the central opening: red, 0; blue, 40; black, 70 mm. Points on curves correspond to conditions for formation of developed shock in the focal waveform. Dotted line shows corresponding dependences of pressure amplitude at the focus in a linear beam.

explained by the change in their area and, accordingly, the aperture. Indeed, when increasing the central opening of the original transducer, the area and aperture of the equivalent source are reduced. The source becomes less focused and consequently the size of its focal region increases, both in the longitudinal and transverse directions (Figs. 3a, 3c, 3d). The trends towards lengthening and, conversely, narrowing of the focal region of ring transducers with increasing the size of the central opening were noted earlier in [31, 32] and can be qualitatively explained as follows. As the size of the opening increases and the width of the ring transducer decreases accordingly, the diffraction divergence of the beam it creates increases. This leads to an increase in the region of intersection of waves arriving with the same phase to the transducer axis from different parts of the ring, i.e., to an extension of the length of the focal region. On the other hand, the larger the size of the opening, the greater the angle at which the waves that arrive in phase to the transducer axis interfere. This leads to a narrowing of the transverse dimensions of constructive interference, which determines the width of the focal region. As follows from solution (13), elongation of the focal region occurs slowly at first, then more rapidly, formally tending to infinity as the size of the opening approaches the size of the original transducer.

Thus, the equivalent source model, constructed in accordance with the above principles, makes it possible to match the axial pressure distributions for the original transducer and the selected equivalent source in a sufficiently wide region around the focus (Fig. 2). However, as the opening size increases, the model yields significant differences in the transverse pressure distributions, indicating the possibility of different manifestations of nonlinear effects at increasing transducer power levels.

2. Effect of Opening Size on the Manifestation of Nonlinear Acoustic Effects

Figure 4 compares the results of numerical modeling of nonlinear operating modes of transducers with the same power, but without an opening and with openings of 40 and 70 mm. The dependences of the peak positive and peak negative pressures, as well as the amplitude of the shock front at the focus on the power of the transducers (saturation curves) are presented. The corresponding dependences of the pressure amplitude at the focus in the absence of nonlinear effects are also given. It is seen that changing the size of the opening leads to significant differences in the dependence of the peak positive pressure and the shock amplitude in the wave profile *versus* transducer power. At the same time, the differences in the dependence of the peak negative pressure *versus* power are substantially weaker.

At low powers, as in a linear beam, the peak positive pressure at the focus increases proportionally to the square root of the power and the area of the transducers (Fig. 4). With further increase in power and corresponding strengthening of nonlinear effects, the peak positive pressure for transducers with larger opening increases at first slower, then, when the shock front is formed (the beginning of steep sections on the curves), it increases faster and reaches higher values at high powers in saturation modes (flattening of the curves).

Power levels, at which a shock front begins to form in the wave profile (the beginning of the dashed curves in Fig. 4) and a developed shock is formed ($p+ = A_{sh}$, marked with dots in Fig. 4), increase with the size of the opening. For example, to achieve the condition of developed shock front at the focus, a power of 635, 745, and 1032 W is required for transducers without an opening and with openings with diameters of 40 and 70 mm, respectively. The intensities on the surfaces of the transducers are 7.4, 10.2, and 22.6 W/cm^2, and the amplitude of the developed shock are A_{sh} = 97, 116, and 145 MPa, respectively. As can be seen from the figure, the shock amplitude in saturation modes also increases with increasing the opening diameter. The observed trends can be explained by the increase in the beam convergence angle created by thinner ring transducers, which leads to less collinear and, thus, less efficient interaction of waves. Similar effects were observed in the fields of transducers without an opening with larger focusing angles [17, 34]. Thus, in terms of manifestation of nonlinear effects, larger central opening in the transducer with a given external aperture (Fig. 1) leads to its operation as being more focused compared to the original.

In Fig. 5, the differences between the wave profiles at the focus for different opening diameters are analyzed in more detail in three typical cases of manifestation of nonlinear effects: in the quasi-linear regime, when 10% of the wave intensity falls on the higher harmonics [17, 33], in the above-considered regime of formation of a developed shock, when the lower boundary of the shock is located at the zero pressure level [17, 34], and in the saturation regime, when the derivative of the peak positive pressure with respect to the pressure at the source $\partial p^+/\partial p_0$ decreases to 10% of the corresponding value for the case of formation of a developed shock [17].

The results in Fig. 5 show that the thresholds of the quasi-linear regime are reached significantly later with increasing opening diameters: the transducer powers are 68, 79, and 109 W (initial intensities of 0.79, 1.08, and 2.38 W/cm^2) for openings with diameters of 0, 40, and 70 mm, respectively. At the same time, the quasi-linear profiles themselves differ only slightly (Fig. 5a). To form a developed shock at the focus, a higher transducer power is also required, the magnitude of the peak positive pressure and amplitude of the shock are significantly higher for transducers with larger opening size, while the peak negative pressures are close in magnitude (Fig. 5b). Saturation regime is also achieved at high powers: 5846, 7063, and 9522 W (the intensity on the transducer is 68, 97, and 208 W/cm^2), the peak positive pressure and the amplitude of the shock front increase with increasing opening size, while the peak negative pressures are only slightly different (Fig. 5c).

Figure 6 shows the spatial distributions of the peak positive and peak negative pressures in the axial plane of the beam for the regimes when a developed shock is formed at the focus of transducers without an opening and with openings of 40 and 70 mm in diameter. As in the case of linear focusing, with increasing size of the opening, the length of the focal region for the peak positive pressure increases, 6.7, 7.8, and 13.3 mm at a level of −6 dB, and the transverse beam width in the focal plane decreases: 0.8, 0.6, and 0.3 mm (Figs. 6a, 6c, 6e). It should be noted that in a nonlinear beam in the regime of formation of a developed shock at the focus, the width of the focal region for the peak positive pressure and the effect of its narrowing are much more pronounced (a decrease by almost three times with an increase in the size of the opening from 0 to 70 mm) compared to a linear beam (a decrease by 30%).

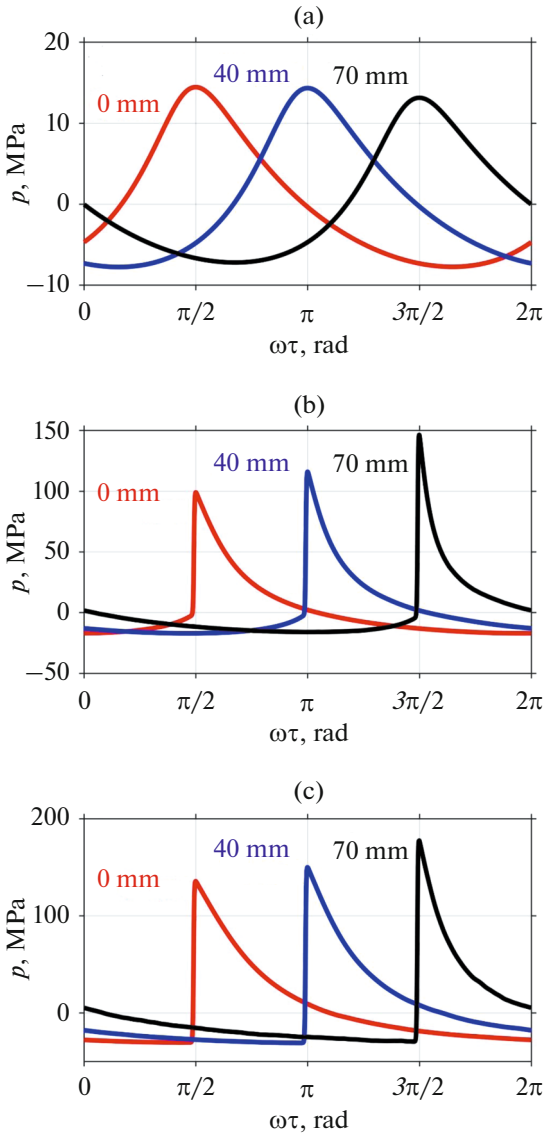

Fig. 5. One cycle of the wave profile at the focus for transducers with different sizes of the central opening: red, 0; blue, 40; black, 70 mm; and different focusing regimes: (a) quasi-linear regime (10% of wave energy in higher harmonics); (b) formation of developed shocks (when lower boundary of the shock front corresponds to zero pressure, $A_{sh} = p+$); (c) saturation regime.

3. Comparison of Ultrasound Fields of Transducers with a Central Opening and Their Equivalent Sources

Figure 7 shows the distributions of the normalized pressure amplitude along the beam axis and across the axis in the focal plane for transducers with central openings with diameters of 10 (left column), 40 (middle column) and 70 mm (right column) and for their equivalent sources in the case of linear focusing, as well as saturation curves at the focus, demonstrating the manifestations of nonlinear effects for the corresponding cases. As noted above, despite the good match of the field distributions along the beam axis around the focus in the case of linear focusing (Figs. 7a–7c), the transverse structure of the field for the original transducer and its equivalent source is different, becoming wider for equivalent sources (Figs. 7d–7f), and such a difference increases with an increase in the diameter of the central opening.

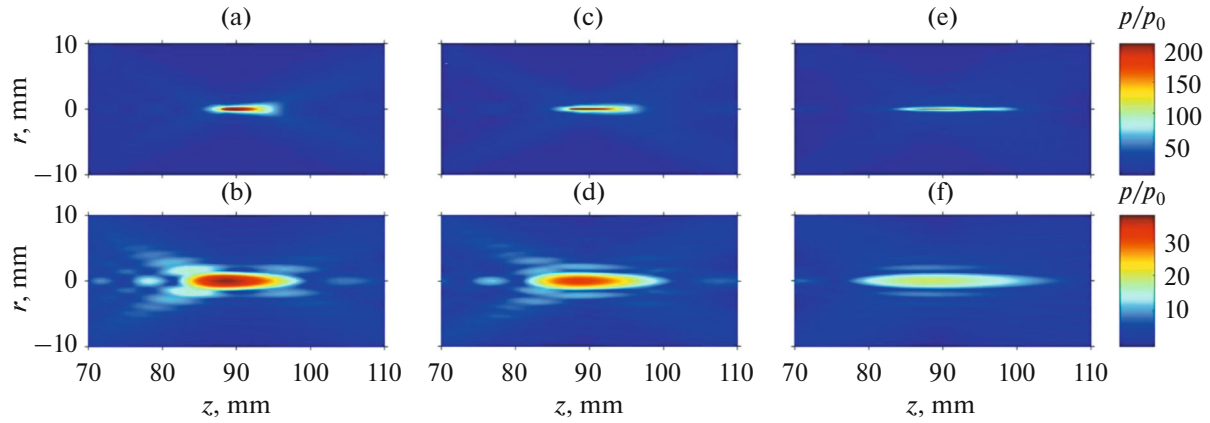

Fig. 6. Distributions of the peak positive (upper row) and peak negative (lower row) pressures in the axial plane of the beam for the case when a developed shock ($A_{sh} = p$) is formed at the focus for different diameters of the central opening: left column, 0; middle column, 40; right column, 70 mm.

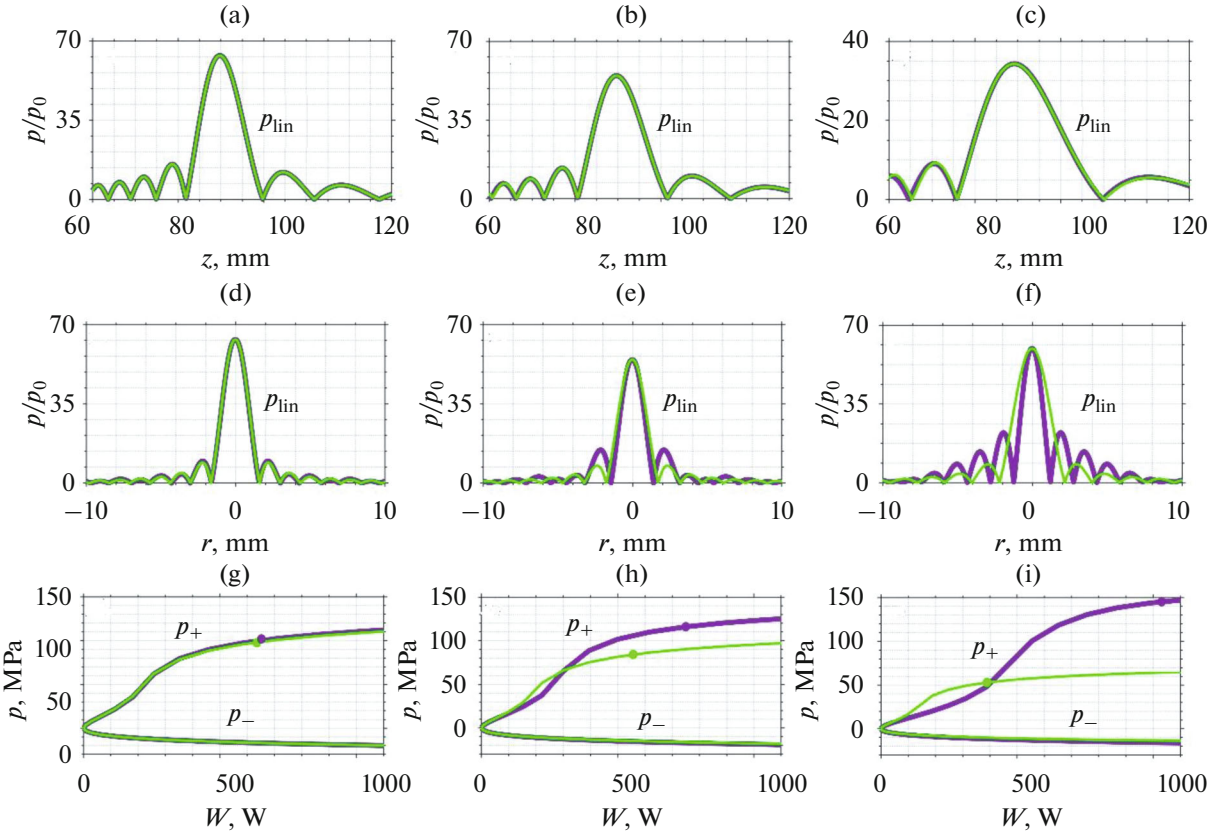

Fig. 7. Comparison of ultrasound field characteristics for transducers with central opening (purple curves) and for their equivalent sources (green curves) for different diameters of the central opening: (a, d, g) 10, (b, e, h) 40, and (c, f, i) 70 mm. Top row: axial distributions of normalized pressure amplitudes in the linear beam. Middle row: transverse distributions of normalized pressure amplitudes in the focal plane of a linear beam. Bottom row: saturation curves for the peak positive and peak negative pressures at the focus; points on curves correspond to formation of developed shock in the focal waveform.

An increase in the opening size also leads to an increase in the discrepancy between the values of the peak positive pressure at the focus of the nonlinear beams (Figs. 7g–7i). Moreover, if for the original transducers the power required to form a developed shock (marked by dots on the curves) increases with increasing opening size—645, 745, and 1032 W—then for the corresponding equivalent sources, on the con-

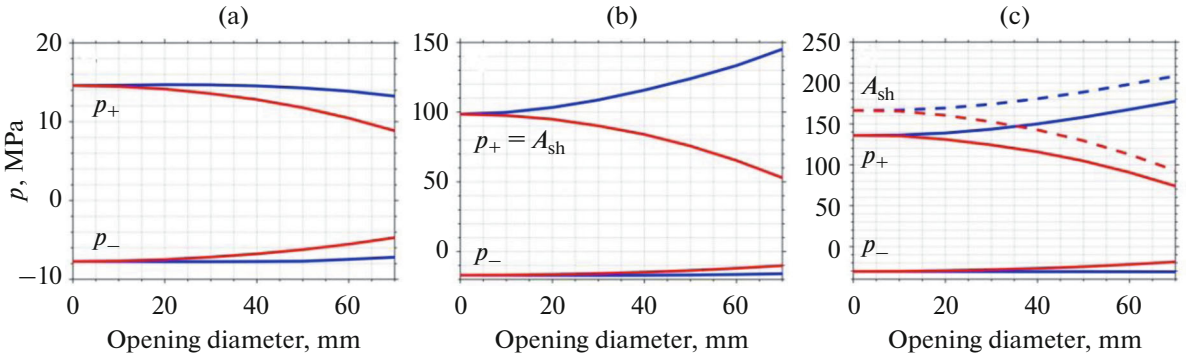

Fig. 8. Dependences of the peak positive and peak negative pressures at the focus on the diameter of a central opening for original transducers (blue curves) and for the corresponding equivalent sources (red curves) for different focusing regimes: (a) quasi-linear; (b) formation of developed shock; (c) saturation regime (shock amplitude is shown by dotted line).

trary, it decreases: 630, 558, and 390 W (Figs. 7g–7i). For the same regime of forming a developed shock at the focus, the peak positive pressures also change differently: they increase (100, 116, and 145 MPa) for the original transducers and decrease (98, 84 and 53 MPa) for the equivalent sources. Thus, for transducers with large opening diameters, the parameters of the nonlinear field at the focus will not correspond to those predicted by the equivalent source model.

Figure 8 shows the dependences of the peak positive and peak negative pressures, as well as the shock amplitude at the focus, on the size of the central opening for the original transducers and their equivalent sources in three characteristic modes of manifestation of nonlinear effects: quasi-linear, formation of a developed shock, and saturation. As noted above, the peak positive pressures differ most significantly from each other, especially in the modes of strong manifestation of nonlinearity (Figs. 8b, 8c). If in the quasi-linear case both dependences decrease monotonically (Fig. 8a), then in cases of formation of a developed shock (Fig. 8b) and saturation (Fig. 8c), the peak positive pressure, as well as the shock amplitude, increase with an increase in the diameter of the opening for the original transducers, but decreases for equivalent sources. A difference of 10% between the curves in the regime of formation of developed shock is achieved with an opening diameter of 22 mm (22% of the transducer diameter). The differences in peak negative pressure values are less significant but also increase with increasing the opening size: p_- increases faster for equivalent transducers, so the waveforms with shocks of ring transducers (Fig. 5) will be more asymmetric compared to those of their equivalent sources.

Thus, the equivalent source model makes it possible to accurately describe nonlinear fields of transducers with a central opening if the opening size is ~20% or less of the transducer diameter. For larger sizes, more precise models must be used.

CONCLUSIONS

The paper analyzes the effect of the size of a central opening in a spherical single-element transducer with a uniform distribution of normal component of vibrational velocity on its surface on the manifestation of nonlinear effects in focused ultrasound beam such transducer creates. It is shown that the presence of a central opening significantly affects the parameters of the nonlinear field in the focal region, leads to a higher effective focusing angle and, therefore, to higher levels of the peak positive pressure and characteristic amplitudes of the shock front in the focal waveform. With an increase in the diameter of the central opening, the beginning of shock formation, formation of a developed shock, and saturation of the pressure field parameters at the focus occur at higher acoustic powers of the transducer.

The limits of applicability of the equivalent source model in the form of a spherical segment for describing the nonlinear field at the focus of a spherical transducer with an opening in the center were determined. It is shown that the condition of equivalence of the linear fields of transducers as a spherical segment without an opening and with a central opening is met when their areas are equal; however, the model can be applied only in the case of relatively small diameters of the central opening. For the transducer considered in this paper with $F_\# = 0.9$ the model is applicable if the diameter of the central opening does not exceed 22% of the transducer diameter. The applicability criterion was a difference in the amplitudes of developed shocks in the focal pressure waveform of less than 10%. As the size of the central opening increases, the simplified equivalent source model becomes unsuitable for describing nonlinear field of the original ring transducer at the focus, so modeling the operation of such transducers requires a more accurate consideration of their geometry.

In a subsequent study, it is planned to generalize the conclusions about the applicability of the equivalent source model for estimating the parameters of

nonlinear fields of spherical transducers with different dimensions relative to the ultrasound wavelength and $F_{\#}$ values.

FUNDING

This study was supported by the Russian Science Foundation, grant no. 20-12-00145 and the Basis Scholarship Foundation stipend no. 24-2-10-21-1.

CONFLICT OF INTEREST

The authors of this work declare that they have no conflicts of interest.

REFERENCES

1. L. R. Gavrilov, *Focused High Intensive Ultrasound in Medicine* (Fazis, Moscow, 2013) [in Russian].
2. M. R. Bailey, V. A. Khokhlova, O. A. Sapozhnikov, S. G. Kargl, and L. A. Crum, Acoust. Phys. **49** (4), 369 (2003).
3. Z. Xu, T. D. Khokhlova, C. S. Cho, and V. A. Khokhlova, Annu. Rev. Biomed. Eng. **26**, 141 (2024).
4. R. P. Williams, J. C. Simon, V. A. Khokhlova, O. A. Sapozhnikov, and T. D. Khokhlova, Int. J. Hyperthermia **40** (1), 1 (2023).
5. Y. S. Kim, B. Keserci, A. Partanen, H. Rhim, H. K. Lim, M. J. Park, and M. O. Köhler, Eur. J. Radiol. **81** (11), 3652 (2012).
6. P. Ramaekers, M. De Greef, J. M. M. Van Breugel, C. T. W. Moonen, and M. Ries, Phys. Med. Biol. **61**, 1057 (2016).
7. J. Kennedy, F. Wu, G. Ter Haar, F. Gleeson, R. Phillips, M. Middleton, and D. Cranston, Ultrasonics **42**, 931 (2004).
8. Yu. S. Andriyakhina, M. M. Karzova, P. V. Yuldashev, and V. A. Khokhlova, Acoust. Phys. **65** (2), 141 (2019).
9. P. A. Pestova, M. M. Karzova, P. V. Yuldashev, and V. A. Khokhlova, Acoust. Phys. **69** (4), 448 (2023).
10. M. S. Canney, V. A. Khokhlova, O. V. Bessonova, M. R. Bailey, and L. A. Crum, Ultrasound Med. Biol. **36** (2), 250 (2010).
11. C. R. Bawiec, T. D. Khokhlova, O. A. Sapozhnikov, P. B. Rosnitskiy, B. W. Cunitz, M. A. Ghanem, C. Hunter, W. Kreider, G. R. Schade, P. V. Yuldashev, and V. A. Khokhlova, IEEE Trans. Ultrason. Ferroelect. Freq. Control **68** (5), 1496 (2021).
12. S. Bobkova, L. Gavrilov, V. Khokhlova, A. Shaw, and J. Hand, Ultrasound Med. Biol. **36** (6), 888 (2010).
13. M. M. Karzova, W. Kreider, A. Partanen, T. D. Khokhlova, O. A. Sapozhnikov, P. V. Yuldashev, and V. A. Khokhlova, IEEE Trans. Ultrason. Ferroelect. Freq. Control **70** (6), 521 (2023).
14. T. D. Khokhlova, G. R. Schade, Y. N. Wang, S. V. Buravkov, V. P. Chernikov, J. C. Simon, F. Starr, A. D. Maxwell, M. R. Bailey, W. Kreider, and V. A. Khokhlova, Sci. Rep. **9**, 20176 (2019).
15. S. A. Tsysar, P. B. Rosnitskiy, S. A. Asfandiyarov, S. A. Petrosyan, V. A. Khokhlova, and O. A. Sapozhnikov, Acoust. Phys. **70** (1), 82 (2024).
16. A. D. Maxwell, P. V. Yuldashev, W. Kreider, T. D. Khokhlova, G. R. Schade, T. L. Hall, O. A. Sapozhnikov, M. R. Bailey, and V. A. Khokhlova, IEEE Trans. Ultrason. Ferroelect. Freq. Control **64** (10), 1542 (2017).
17. P. B. Rosnitskiy, P. V. Yuldashev, O. A. Sapozhnikov, A. D. Maxwell, W. Kreider, M. R. Bailey, and V. A. Khokhlova, IEEE Trans. Ultrason. Ferroelect. Freq. Control **64** (2), 374 (2017).
18. M. S. Canney, M. R. Bailey, L. A. Crum, V. A. Khokhlova, and O. A. Sapozhnikov, J. Acoust. Soc. Am., No. 4, 2406 (2008).
19. O. A. Sapozhnikov, S. A. Tsysar, V. A. Khokhlova, and W. Kreider, J. Acoust. Soc. Am. **138** (3), 1515 (2015).
20. W. Kreider, P. V. Yuldashev, O. A. Sapozhnikov, N. Farr, A. Partanen, M. R. Bailey, and V. A. Khokhlova, IEEE Trans. Ultrason. Ferroelectr. Freq. Control **60** (8), 1683 (2013).
21. M. M. Karzova, P. V. Yuldashev, O. A. Sapozhnikov, V. A. Khokhlova, B. W. Cunitz, W. Kreider, and M. R. Bailey, J. Acoust. Soc. Am. **141** (4), 2327 (2017).
22. P. V. Yuldashev and V. A. Khokhlova, Acoust. Phys. **57** (3), 334 (2011).
23. J. Gu and Y. Jing, IEEE Trans. Ultrason. Ferroelectr. Freq. Control **62** (11), 1979 (2015).
24. J. E. Soneson, Proc. AIP Conf. **1113** (1), 165 (2009).
25. P. V. Yuldashev, M. M. Karzova, W. Kreider, P. B. Rosnitskiy, O. A. Sapozhnikov, and V. A. Khokhlova, IEEE Trans. Ultrason. Ferroelectr. Freq. Control **68** (9), 2837 (2021).
26. P. B. Rosnitsky, P. V. Yuldashev, B. A. Vysokanov, and V. A. Khokhlova, Acoust. Phys. **62** (2), 151 (2016).
27. E. M. Ponomarchuk, P. V. Yuldashev, D. A. Nikolaev, S. A. Tsysar, A. A. Mironova, and V. A. Khokhlova, Acoust. Phys. **69** (4), 459 (2023).

28. P. B. Rosnitskiy, S. A. Tsysar, M. M. Karzova, S. V. Buravkov, P. G. Malkov, N. V. Danilova, E. M. Ponomarchuk, O. A. Sapozhnikov, T. D. Khokhlova, G. R. Schade, A. D. Maxwell, Y. N. Wang, A. V. Kadrev, A. L. Chernyaev, D. A. Okhobotov, A. A. Kamalov, and V. A. Khokhlova, Ultrasonics **133**, 107029 (2023).

29. T. Khokhlova, P. Rosnitskiy, C. Hunter, A. Maxwell, W. Kreider, G. Ter Haar, M. Costa, O. Sapozhnikov, and V. Khokhlova, J. Acoust. Soc. Am. **144** (3), 1160 (2018).

30. H. T. O'Neil, J. Acoust. Soc. Am. **21** (5), 516 (1949).

31. K. Beissner, J. Acoust. Soc. Am. **131** (1), 620 (2012).

32. K. Beissner, J. Acoust. Soc. Am. **134** (5), 3943 (2013).

33. *Ultrasonics-Field Characterization – in Situ Exposure Estimation in Finite-Amplitude Ultrasonic Beams, Document IEC/TS 61949* (2007).

34. P. B. Rosnitsky, P. V. Yuldashev, and V. A. Khokhlova, Acoust. Phys. **61** (3), 301 (2015).